Thin Solid Films 518 (2010) 2050–2055

Contents lists available at ScienceDirect

Thin Solid Films

journal homepage: www.elsevier.com/locate/tsf

Deposition and characterisation of $MoSi_2$ films

J.V. Rau [a,*], R. Teghil [b], D. Ferro [c], A. Generosi [a], V. Rossi Albertini [a], M. Spoliti [d], S.M. Barinov [e]

[a] Istituto di Struttura della Materia, CNR, via del Fosso del Cavaliere 100-00133 Rome, Italy
[b] Università della Basilicata, Dipartimento di Chimica, via N. Sauro 85-85100, Potenza, Italy
[c] Istituto per lo Studio dei Materiali Nanostrutturati, CNR, Piazzale Aldo Moro 5-00185 Rome, Italy
[d] "Sapienza" Universitá di Roma, Dipartimento di Chimica, Piazzale Aldo Moro 5-00185 Rome, Italy
[e] Baikov Institute of Metallurgy and Materials Science, Russian Academy of Sciences, Leninskij prospect 49-119991 Moscow, Russia

ARTICLE INFO

Article history:
Received 27 November 2008
Received in revised form 16 September 2009
Accepted 21 September 2009
Available online 2 October 2009

Keywords:
Molybdenum disilicide
Coatings
Pulsed laser deposition
Hardness
X-ray Diffraction

ABSTRACT

Deposition of $MoSi_2$ films on silicon and tantalum substrates applying pulsed laser deposition technique has been performed. Crystalline, hexagonal symmetry, $MoSi_2$ films were prepared directly from stoichiometric $MoSi_2$ tetragonal target on room temperature and heated substrates (500 °C). Textured $MoSi_2$ films having privileged (110) and (115) orientations and average crystallite size of about 105 nm were grown on Si(111) substrates with a good degree of axial texture (rocking curve full width half maximum of 1.5°). $MoSi_2$ films grown on Ta(211) substrates, instead, turned out to be polycrystalline, with an average crystallite size of about 100 nm and 50 nm on substrates kept at room temperature and at 500 °C, respectively. Vickers hardness for 1.2 μm thick $MoSi_2$ films on Si(111) substrates resulted to be 15 GPa both at room temperature and 500 °C, while for 0.4 μm thick $MoSi_2$ films on Ta(211) substrates — 26 GPa at room temperature and 30 GPa at 500 °C.

1. Introduction

Molybdenum disilicide ($MoSi_2$) is a borderline intermetallic compound, which belongs to a group of high temperature structural silicides. It possesses a combination of special properties such as high melting point (≈2030 °C), low density, "ceramic-like" excellent high temperature oxidation resistance (up to 1600 °C) and "metal-like" plasticity at elevated temperatures, along with a high thermal conductivity. Furthermore, $MoSi_2$ is a relatively low cost, non toxic and environmentally benign material. Another attractive feature of $MoSi_2$ is that it can be metallurgically alloyed with silicides to further improve its properties. Materials based on $MoSi_2$ have a variety of industrial and aerospace applications, including heating elements for furnaces operating at temperatures up to 1800 °C, power generation components, turbine aircraft engine hot section components, etc. [1–4]. It is also known to be a lubricant, battery cathode and catalyst.

Among the drawbacks of monolithic $MoSi_2$ are high brittleness, and low strength and creep resistance at high temperatures. $MoSi_2$ bulk Vickers hardness is low, about 11.3 GPa [5]. A way to overcome these problems could be the application of various $MoSi_2$ composites possessing improved properties [1–3,6,7] or, alternatively, the application of $MoSi_2$ in the form of thin films. Due to the excellent oxidation resistance $MoSi_2$ is a good candidate for protective coatings. Moreover, $MoSi_2$ thin films are of interest in microelectronic applications for gates, contacts, interconnects and diffusion barriers [8].

Several deposition processes have been tried to produce $MoSi_2$ thin films, among them sputtering [9,10], chemical vapour deposition [11,12] and pulsed laser deposition [13]. The available literature data are related mainly to $MoSi_2$ films deposited on Si substrates. We report here the $MoSi_2$ deposition also on tantalum substrates, which could have an important input for industry. Tantalum is characterized by a high melting point (about 3000 °C) and a high corrosion resistance. It shares with $MoSi_2$ some characteristics that allow its broad application in various technological fields, such as material for heating elements and for furnaces operating above 1700 °C, as well as anode material. However, hardness of pure tantalum is rather low 0.9–1.5 GPa. Furthermore, upon heating over 300 °C, Ta oxidises forming a porous layer of Ta_2O_5 on its surface. To improve the resistance to high temperature, it could be coated with a more inert material, like, for instance, $MoSi_2$.

This study is aimed at the characterization of pulsed laser deposited $MoSi_2$ films on Si and Ta substrates. Morphological and structural characterizations of the films were carried out by Scanning Electron Microscopy (SEM) coupled with a system for microanalysis (Energy Dispersive X-Ray Spectroscopy (EDXRS)) and Energy Dispersive X-Ray Diffraction (EDXRD). Vickers hardness data on $MoSi_2$ films on the above mentioned substrates are reported.

2. Experimental details

2.1. Materials

Rectangular 10×10 mm specimens of Si(111) slabs (1 mm thick) and of Ta(211) foil (0.5 mm thick) were used as substrates. $MoSi_2$

* Corresponding author. Tel.: +39 06 4991 3641; fax: +39 06 4991 3951.
E-mail address: giulietta.rau@uniroma1.it (J.V. Rau).

0040-6090/$ – see front matter © 2009 Elsevier B.V. All rights reserved.
doi:10.1016/j.tsf.2009.09.087

powder (99.9% purity) was purchased from Cerac company. To obtain a $MoSi_2$ monolithic target, the powder was hot pressed in Argon atmosphere under the following conditions: 30 MPa, 1720 °C, 10 min. According to the X-ray Diffraction analysis the target consisted of the tetragonal $MoSi_2$ phase with a negligible admixture of Mo_5Si_3 phase. SEM-EDXRS studies confirmed this result and showed the target to be formed by pure and stoichiometric $MoSi_2$ phase: 63 wt.% of Mo and 37 wt.% of Si. Depositions were performed at two substrate temperatures: room (RT) and 500 °C.

2.2. Methods

2.2.1. Pulsed laser deposition

The experimental apparatus has been described in details elsewhere [14]. Shortly, the ablation laser source is a frequency doubled Nd: YAG laser ($\lambda = 532$ nm, $E = 2.5$ mJ, repetition rate = 10 Hz, the laser pulse duration (10 ns)). The substrate was kept at a distance of 2 cm from the $MoSi_2$ target. The deposition time was 2 h. All the experiments were carried out in high vacuum (4×10^{-4} Pa).

2.2.2. Energy Dispersive X-ray Diffraction analysis

The EDXRD measurements were executed by a non-commercial machine [15], based on the use of a polychromatic ("white") primary X-ray beam produced by a W anode tube, and of an ultrapure Ge solid-state detector, which allows to accomplish the energy scan of the diffracted photons. In this way, the reciprocal space scan (or q-scan, $q = aE\sin\vartheta$, where q is the normalized momentum transfer magnitude, a is a constant, E is the energy of the incident X-ray beam and 2ϑ is the scattering angle), necessary to collect the diffraction pattern, is carried out electronically, rather than mechanically, as in the conventional Angular Dispersive X-Ray Diffraction method. The main advantage of the Energy Dispersive (ED) mode for X-Ray Diffraction studies is that the experimental setup is kept fixed during the pattern acquisition. The energy resolution is about 1.5%, while the maximum count rate — 10 kcounts/s. Source and detector arms are moved by two linear actuators driven by step motors, leading to a minimum scattering angle increment of 0.004°.

The same experimental setup was used to perform the investigations of the structural properties of all the film samples, including the measurements of their Rocking Curves (RC) [16]. The RC of a polycrystal represents the statistical distribution of the orientation of its crystalline domains. The RC measurement requires the collection of the intensity of a given Bragg peak as a function of the asymmetry parameter $\alpha = (\vartheta i - \vartheta r)/2$, while the total scattering angle $(\vartheta i + \vartheta r) = 2\vartheta$ is kept unchanged: in these conditions, the RC corresponds to the Bragg peak intensity vs. α curve, normalized to its maximum value along the α scan. Moreover, when RC measurements are performed the EDXRD mode is particularly efficient, since all Bragg peaks present in the selected q-region are collected simultaneously. This allows the acquisition of the RCs of all the visible reflections, thus providing richer statistical information on sample structure and texture.

The main advantage of the ED mode over its conventional counterpart in performing X-ray Diffraction experiments is that the geometric setup is kept fixed during the acquisition of the diffraction patterns, which simplifies the experimental geometry and prevents systematic angular errors, as well as possible misalignments. In particular, this technique provides a faster recording of the Bragg peaks and, consequently, of their RCs since, in the ED mode, the whole diffraction pattern is obtained in parallel at any q-value.

Preliminary measurements were performed to choose the ideal scattering angle in order to explore the q-range of interest (containing both the substrate and most of the polycrystalline molybdenum silicide Bragg reflections) and the optimized working conditions were found to be as follows: $E = 55$ keV, $I = 15$ mA and scattering angle $2\vartheta = 11.5°$. This preliminary set up was chosen to perform all the diffraction measurements, in reflection mode, and to collect the RCs of all the film samples.

2.2.3. Scanning Electron Microscopy analysis

Scanning Electron Microscopy (a LEO 1450 Variable Pressure apparatus), working in secondary and backscattered electron modes, was utilized for morphological studies of the deposited $MoSi_2$ films. Our SEM apparatus is coupled with a system for microanalysis (EDXRS) INCA 300 that allows executing qualitative/quantitative analysis of the elements. The plane and cross-section view images were obtained, the latter being necessary for the thickness measurements of films. Since the images of the films thickness were obtained at the sample edge tilted by 45°, the measured values were multiplied by $\sqrt{2}/2$.

2.2.4. Vickers hardness measurements

The microhardness measurements were carried out by means of a Leica VMHT apparatus (Leica GmbH, Germany) equipped with a standard Vickers pyramidal indenter (square-based diamond pyramid of 136° face angle). The loading and unloading speed was 5×10^{-6} m/s, and the time under the peak load was 15 s. Hardness of the substrates, bulk target and the deposited films were measured according to the procedure described in detailed in our previous works [17,18].

For film samples, the measured hardness was that of the film/substrate composite system. To separate the composite hardness of the film/substrate system (H_c) on its components, film (H_f) and substrate (H_s), a Jönsson and Hogmark model based on area "law-of-mixtures" approach was applied [19], taking into account the indentation size effect [20]. In this case, composite hardness H_c is expressed as:

$$H_c = H_{s0} + [B_s + 2ct(H_{f0} - H_{s0})]/D, \quad (1)$$

where $c \cong 0.5$ for a brittle hard film on a more ductile substrate [19]; H_{s0} and H_{f0} are the intrinsic hardness of substrate and film, respectively; t is film thickness; D is the imprint diagonal, and B_s is the coefficient, which is determined from substrate hardness measurements.

To evaluate H_{s0} and B_s values, hardness of the Si(111) and Ta(211) substrates was measured separately. The relation between the measured substrate hardness, H_s, and the reciprocal length of the indentation imprints is expressed by the following equation [21]:

$$H_s = H_{s0} + B_s/D. \quad (2)$$

The values obtained for the Si(111) substrate hardness, H_{s0} and the B_s coefficient, equal to 9.4 ± 0.4 GPa and $(17.3 \pm 2.9)\times10^{-6}$ GPa m, respectively, while for Ta(211) substrate, H_{s0} and B_s, equal to 1.0 ± 0.1 GPa and $(5.9 \pm 0.5)\times10^{-6}$ GPa m, respectively.

To calculate the intrinsic hardness of the films, special attention was paid to choose correctly the indentation depths, $d = D/7$ (for Vickers pyramidal indenter), i.e. in the interval, where the applied model is adequate. The $d/t (= D/7t)$ range for $MoSi_2$film/Si(111) substrate system is (0.9–2.0), while for $MoSi_2$film/Ta(211)substrate system is (1.5–14.6), both being perfectly in the range of substrate-dominated mixed region, where the film is fractured conforming to the plastically deforming substrate [22]. In this d/t range, the results obtained using the Jönsson and Hogmark model have been demonstrated to coincide well with the estimations resulting from more complicated models [22,23].

For the $MoSi_2$ bulk target hardness measurements, indentations were made with 5 loads ranging from 1 to 10 N. On each $MoSi_2$/Si sample indentations were made with 3 loads ranging from 0.5 to 2 N, while on $MoSi_2$/Ta samples — with 3 loads ranging from 0.3 to 1 N. The indentations at higher loads led to the imprint cracking. For all the samples the number of indentations made at each load was approximately 10–15.

3. Results and discussion

EDXRD measurements were performed on a series of thin films deposited from $MoSi_2$ target upon monocrystalline Si(111) and Ta (211) at RT and 500 °C. The aim of these diffraction measurements was to detect the stoichiometric composition of the deposited films and their crystalline/amorphous nature. In Fig. 1, the EDXRD patterns collected on the molybdenum silicide films on Si(111) substrates are shown shifted in intensity to make the comparison at various temperatures easier. Our pulsed laser deposited films exhibited hexagonal symmetry, while the starting material was tetragonal $MoSi_2$. Several Bragg reflections attributable to the formation of $MoSi_2$ film (Sys: hexagonal, S.G. $P6_222(180)$ [24]) were detected. Both the films, grown at different substrate temperatures, present the same crystallographic structure, no shift nor intensity variation being detected analysing the $MoSi_2$ Bragg reflections. Moreover, for the film grown at 500 °C three more peaks were observed, consistent with the formation of a polycrystalline MoO_2 layer, characterized by randomly oriented grains, the oxidation process being likely induced by the high temperature. Comparing these results with the crystallographic data for the $MoSi_2$ polycrystalline powder, it turns out that the relative intensities of the Bragg peaks in the diffraction patterns do not correspond to a random distribution of the crystal domains (powder-like). It can be noticed that the $MoSi_2(115)$ peak (11% relative intensity in the powder diffraction database), turns out to be the most intense reflection, while the $MoSi_2(111)$ (100% relative intensity) is completely missing.

Based on these observations, a hypothesis, concerning the preferential orientation and the film texture along the $MoSi_2(110)$ and (115) crystallographic directions, can be made. To validate this hypothesis, the rocking curve analysis was performed. As discussed above, the RC of a polycrystal represents the statistical distribution of the crystallites orientation. This analysis was carried out for both the films in the same asymmetry range ($-1.2° < \alpha < 1.2°$). In Fig. 2, the results of the $MoSi_2$ RC analysis are shown together with the RC of the Si(111) substrate (triangles), which was used as an internal reference. In the upper part of the figure (film deposited at RT), the rocking curves obtained by the analysis of the most intense $MoSi_2(110)$ (hollow dots) and (115) (filled dots) reflections are shown. The evaluation of the full width half maximum (FWHM) of the Gaussian fit of these RCs confirmed a moderate texture of the film ($FWHM_{(110)\ RT} = 1.5° \pm 0.1°$ and $FWHM_{(115)\ RT} = 1.7° \pm 0.1°$, respectively). Moreover, the film is grown with a certain mismatch with respect to the substrate ($0.5° \pm 0.1°$), as deduced by the angular distance between the $MoSi_2$ RCs maxima and the Si(111) RC maximum.

In the lower part of Fig. 2, the same RC analysis accomplished on $MoSi_2$ film grown at 500 °C is reported. As visible, the RCs corresponding

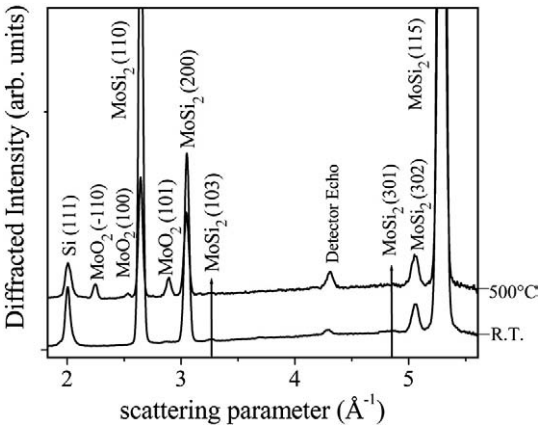

Fig. 1. EDXRD patterns collected upon $MoSi_2$/Si(111) crystalline films deposited at RT (lower pattern) and 500 °C (upper pattern), respectively.

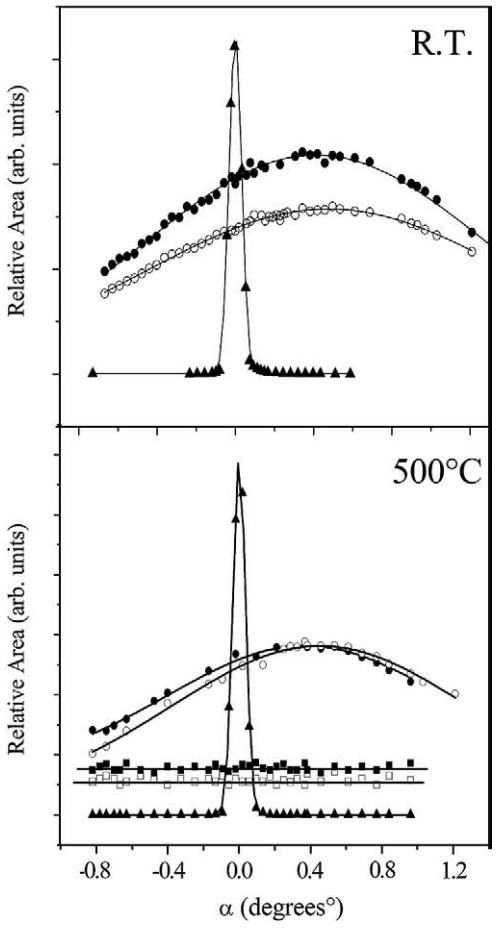

Fig. 2. Rocking curve analysis of crystalline reflections representative of Si(111) substrate and the $MoSi_2$ film grown at room (upper graph) and 500 °C (lower graph). The experimental points are labelled as follows: Si(111) — triangles; $MoSi_2(110)$ — hollow dots; $MoSi_2(115)$ — filled dots; $MoO_2(110)$ — filled squares and $MoO_2(101)$ — hollow squares.

to the Si(111) substrate, and to the $MoSi_2(115)$ (filled dots) and $MoSi_2$ (110) (hollow dots) overlap satisfactory with those of the RT grown film, the numerical values being $FWHM_{(110)\ 500\,°C} = 1.5° \pm 0.1°$ and $FWHM_{(115)\ 500\,°C} = 1.6° \pm 0.1°$.

Moreover, the RC analysis was also performed on the MoO_2 peaks in order to confirm that these reflections can actually be attributed to a textureless surface oxide. Indeed, as visible in Fig. 2, the reported RCs ($MoO_2(110)$ filled squares and $MoO_2(101)$ hollow squares) do not show any preferred orientation of the grains, the distribution of the relative intensities being flat.

The EDXRD measurements upon molybdenum silicide films deposited on monocrystalline Ta(211) substrate were performed under the same experimental conditions described above. In Fig. 3, the patterns collected from these films are shown, the lower spectra corresponding to the RT film, while the upper — to the 500 °C grown film. Both patterns correspond to $MoSi_2$ (Sys: hexagonal, S.G. $P6_222(180)$) films. However, significant differences can be noticed while comparing the spectra. The diffraction pattern collected from the RT grown film evidences that the $MoSi_2(115)$ reflection is the most intense and only a few other diffraction peaks can be detected. For the 500 °C film, all the most intense $MoSi_2$ diffraction peaks are present and their relative intensities are in good agreement with the corresponding powder theoretical diffraction pattern, indicating that a truly polycrystalline $MoSi_2$ film has grown [24]. However, at 500 °C more intense and sharp reflections were expected, since higher temperature usually facilitates the crystallite growth enhancing the diffracted intensity and diminishing the full width half maximum of the peaks.

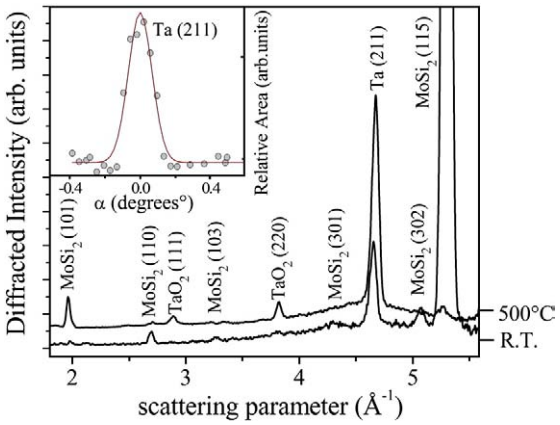

Fig. 3. EDXRD patterns collected upon $MoSi_2$/Ta(211) crystalline films deposited at RT (lower pattern) and 500 °C (upper pattern), respectively.

Furthermore, traces of TaO_2, whose formation was likely induced by the high temperature, were detected. The tantalum dioxide peaks are labelled in Fig. 3 according to [24].

The accurate rocking curve analysis upon RT and 500 °C grown $MoSi_2$/Ta films demonstrated that the films are characterized by a random distribution of the crystallites contributing to the diffracted signal, flat RCs being observed for all the reflections in the explored asymmetry parameter range. In the inset of Fig. 3 the RC of the substrate only, Ta (211), is plotted (FWHM = 0.13° ± 0.02°). It exhibits a lower texture than the Si(111) substrate (FWHM = 0.07 ° ± 0.02°). The RC analysis was also performed on the TaO_2 peaks, confirming the random orientation of its grains.

The $MoSi_2$ crystallites average size was calculated from the Laue equations, which lead to a relation equivalent to the Scherrer formula, but more suitable for the ED mode:

$$\frac{1}{2}tq_1 = (n-1)\pi \text{ and } \frac{1}{2}tq_2 = (n+1)\pi. \quad (3)$$

Combining these equations the average crystallite diameter (in the peak triangular shape approximation) $t = 4\pi/\Delta q \cong 2\pi/\sigma_{[hkl]}$, where $\sigma_{[hkl]}$ is the standard deviation of the [*hkl*] peak, obtained by its Gaussian fit [25]. From $\sigma_{[hkl]}$ the average crystallite size can be evaluated. The $MoSi_2$(110) and (115) crystallites grown onto Si(111) resulted to be (105 ± 5) nm, regardless of the growing temperature. However, on the Ta(211) substrate the average size of the crystallites decreases from (100 ± 5) nm at RT to (50 ± 5) nm for the film grown at 500 °C. This grain size reduction is in agreement with the reduced $MoSi_2$ diffracted intensity observed at 500 °C.

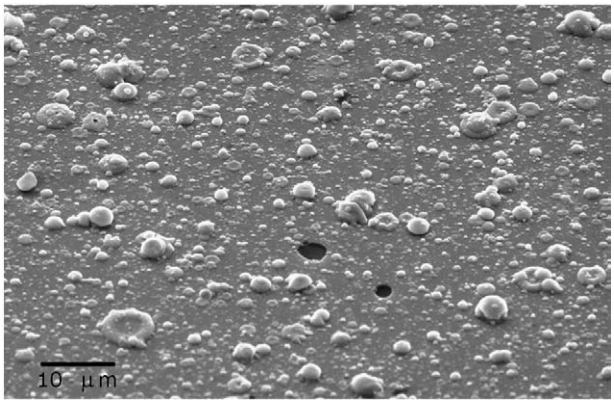

Fig. 4. SEM micrograph of $MoSi_2$ film on Si substrate at RT.

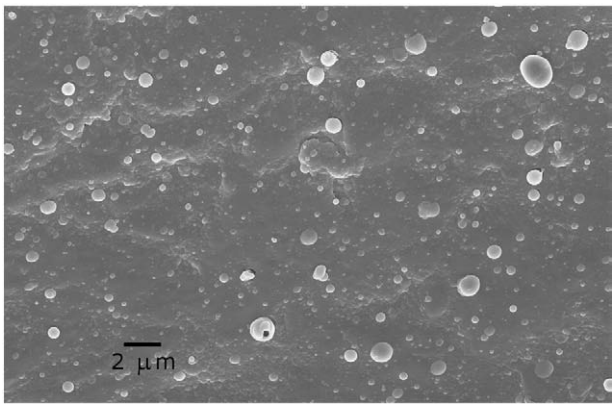

Fig. 5. SEM micrograph of $MoSi_2$ film on Ta substrate at 500 °C.

In all the samples studied no shift of the $MoSi_2$ peaks and, consequently, no stress induced by the temperature have been registered.

SEM micrographs of films are shown in Figs. 4 and 5 (plane view) and in Fig. 6 (cross-section view). All the prepared films have smooth and compact morphology, exhibiting a tight resemblance regardless of the substrate material and deposition temperature. Droplets of a very broad range of size, from about 0.1 µm to almost 10 µm, likely originated from the expulsion of the target, are present on the film surface, being distributed uniformly throughout the surface area. The presence of these droplets and their size range are independent on the substrate material and temperature.

As estimated by the SEM cross-sectional observation, thickness of the $MoSi_2$/Si films is 1.2 ± 0.2 µm, and that of the $MoSi_2$/Ta films is 0.4 ± 0.1, approximately. In our earlier work [26] we reported that during $MoSi_2$ target laser ablation, the plasma contains $(MoSi_2)n$ (n up to 2) clusters together with Si and Mo atoms. Therefore, such a difference in the film thickness under equal deposition conditions could be explained by a partial dissolution of silicon in the Ta substrate, lowering in this way the film thickness in the $MoSi_2$/Ta system. At the same time, silicon cannot be dissolved in the Si substrate of the $MoSi_2$/Si system, resulting in a thicker film deposition.

According to the SEM-EDXRS analysis data, our pulsed laser deposited films contain about 56 wt.% of Mo and 44 wt.% of Si (average values throughout the film surface), the amount of silicon in the films being slightly higher than its stoichiometric amount in a $MoSi_2$ compound (37 wt.%). The droplets contain slightly higher amount of Mo — about 59 wt.%. In the films deposited at 500 °C substrate temperature, the presence of small amount of oxygen was also detected: about 1–3 wt.% for the films on Si(111) substrates, and about 5 wt.% — on Ta(211) substrates. These results are in agreement

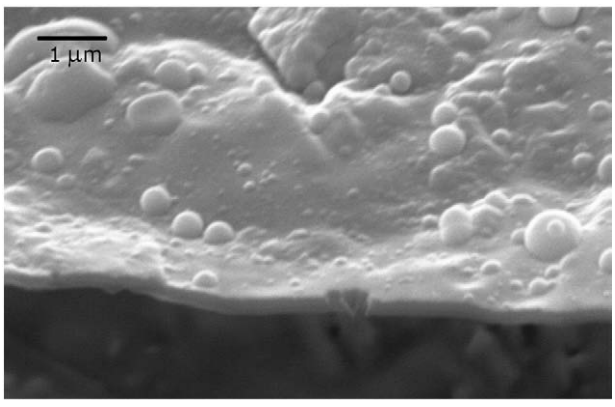

Fig. 6. SEM micrograph of $MoSi_2$ film on Ta substrate at RT: cross-section view.

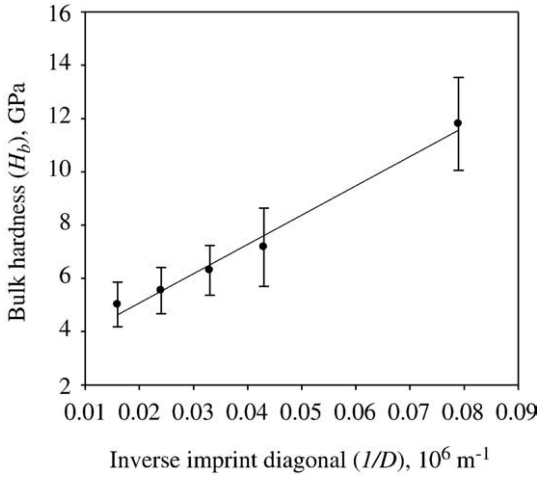

Fig. 7. Vickers hardness of $MoSi_2$ bulk versus inverse imprint diagonal.

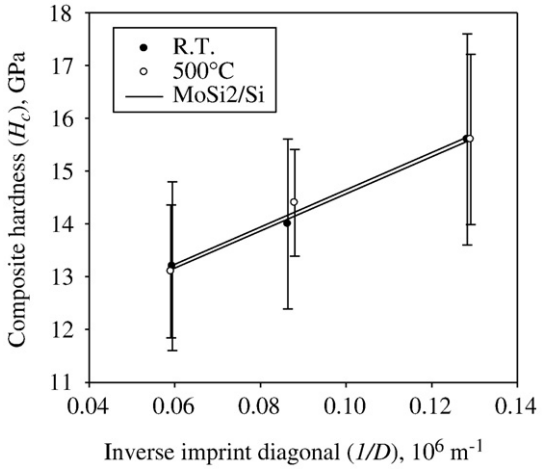

Fig. 8. Composite Vickers hardness of $MoSi_2$ film/Si substrate system versus inverse imprint diagonal.

with those of the EDXRD measurements, which registered the formation of molybdenum dioxide in the case of the Si(111) substrate film, and of tantalum dioxide in the case of the Ta(211) substrate film. Taking into account both the SEM-EDXRS and EDXRD results, one can conclude that the films are composed of $MoSi_2$ mainly, with a not significant amount of amorphous Si and with small amounts of oxides, these latter constituents being registered only for films deposited at 500 °C.

In Fig. 7, the experimental data on Vickers hardness of $MoSi_2$ bulk target versus the inverse imprint diagonal are presented. The average bulk hardness increased from 5.0 ± 0.8 GPa under 9.8 N (1000 g) of load to the maximum of 11.8 ± 1.7 GPa under 1.0 N (100 g) of load. These values are not in contradiction with those reported in the literature [5,26], a rigorous comparison being complicated due to different sintering conditions of monolithic $MoSi_2$ preparation. It was observed that the hardness of monolithic $MoSi_2$ decreases with the increase in the sintering temperature [27], as shown in Table 1, where literature data [27] and our results are presented. Authors [5] report for $MoSi_2$, a bulk hardness of 11.3 GPa under 1 N of load, which is in good agreement with our results, despite the sintering conditions were different (15 MPa at 1400 °C for 24 h). The Vickers hardness of $MoSi_2$ sintered bulk of 8.8 GPa under 9.8 N of load was reported by the authors [6], their value being higher than our experimental result 5.0 ± 0.8 GPa under the same load.

All the mentioned above literature hardness values for $MoSi_2$ bulk are related to the tetragonal phase. In Ref. [28], the results of the first-principles density functional theory calculations, reporting calculated Vickers hardness of the hexagonal $MoSi_2$ phase as 10 GPa, are presented.

In Figs. 8 and 9, the experimental data on the composite film/substrate hardness (H_c) versus the inverse imprint diagonal ($1/D$) for all the four films are presented. The plots were well approximated by linear regressions. Calculated intrinsic hardness values for $MoSi_2$ films on Si(111) and Ta(211) substrates under study are given in Table 2.

It should be noted also that the presence of droplets up to almost 10 μm of diameter on the film surface influenced and complicated the hardness measurements, since the minimum average imprint diagonal (D) resulted to be comparable with the droplet's diameter, being about 8 μm in the case of the $MoSi_2$/Si system and about 5 μm in the case of the $MoSi_2$/Ta system under the lowest load. This led to the enlargement of the composite hardness of the film/substrate system and, consequently, of the intrinsic film hardness range, specially at low loads. At high loads, for the $MoSi_2$/Ta system this phenomenon is not present, since the average D value reaches 41 μm, being much larger than the biggest droplets. In the case of the $MoSi_2$/Si system, the average D range is 8–17 μm and thus, even at high loads, this effect is present.

As one can see from Table 2, the intrinsic $MoSi_2$ films hardness on Si(111) substrates (15 GPa) is somewhat higher, while $MoSi_2$ films hardness on Ta(211) substrates (26–30 GPa) is much higher than that of the $MoSi_2$ bulk. Likely, the enhanced hardness in the latter case could be justified by much smaller film thickness (0.4 μm). The increased hardness for thinner films was also registered in our previous studies for TiC films on titanium substrate [17].

For the $MoSi_2$/Si system, no substrate temperature dependence on hardness was observed, while for the $MoSi_2$/Ta system, the films deposited at 500 °C are harder than those deposited at RT. This latter result regarding the enhanced hardness of the $MoSi_2$ films on Ta substrate, and the data obtained by EDXRD, registering two times decrease in the average crystallite size from 100 nm at RT to 50 nm at

Table 1
Vickers hardness of $MoSi_2$ bulk at different sintering temperatures (applied load is 1.0 N).

Temperature, °C	Hardness, GPa	Literature
1150	14.0	[27]
1300	13.1	[27]
1450	12.4	[27]
1720	11.8	our data

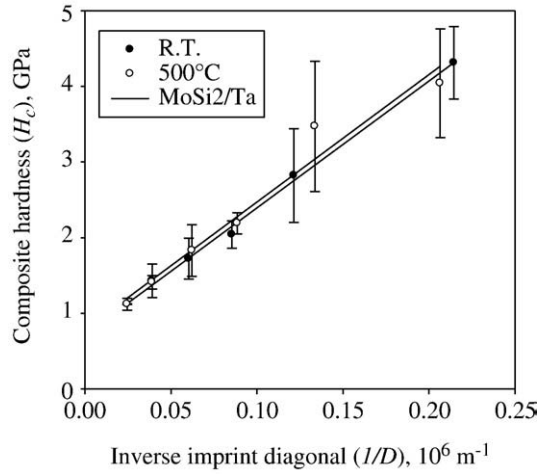

Fig. 9. Composite Vickers hardness of $MoSi_2$ film/Ta substrate system versus inverse imprint diagonal.

Table 2
Hardness of $MoSi_2$ films on Si(111) and Ta(111) substrates.

Film/substrate system	Substrate temperature	Thickness, μm	Vickers hardness, GPa
$MoSi_2$/Si	Room	1.2 ± 0.2	15 ± 6
$MoSi_2$/Si	500 °C	1.2 ± 0.2	15 ± 5
$MoSi_2$/Ta	Room	0.4 ± 0.1	26 ± 3
$MoSi_2$/Ta	500 °C	0.4 ± 0.1	30 ± 4

500 °C, are in agreement with literature [29], reporting that for intermetallics the transition to a nanocrystalline state is accompanied by an increase of hardness.

4. Conclusions

Stoichiometric $MoSi_2$ films on Si(111) and Ta(211) substrates were prepared by pulsed laser deposition technique. The deposition at room and 500 °C substrate temperatures led to the formation of crystalline films with hexagonal symmetry. Moderately textured $MoSi_2$ films with privileged (110) and (115) orientations were grown on Si(111) substrates both at RT and 500 °C, the average degree of axial texture being $FWHM_{(hkl)} \cong 1.5°$. At 500 °C, the formation of disordered polycrystalline MoO_2 was detected. The average crystallite size for the $MoSi_2$ films on Si substrates is about (105 ± 5) nm, independently of the substrate temperature.

The films grown on Ta(211) substrates both at RT and 500 °C are composed of polycrystalline $MoSi_2$. At high temperature, the formation of disordered TaO_2 was detected. The average crystallite size is about (100 ± 5) nm at RT and about (50 ± 5) nm at 500 °C.

Deposited $MoSi_2$ films are harder than the corresponding bulk material. Vickers hardness for 1.2 μm thick $MoSi_2$ films on Si(111) substrates is about 15 ± 6 GPa both at room temperature and 500 °C; while for 0.4 μm thick $MoSi_2$ films on Ta(211) substrates is 26 ± 3 GPa at room temperature and 30 ± 4 GPa at 500 °C.

Acknowledgment

Authors are grateful to Dr. A. Latini for performing the Angular Dispersive X-Ray Diffraction analysis of the $MoSi_2$ target.

References

[1] A.K. Vasudevan, J.J. Petrovic, Mater. Sci. Eng. A 155 (1992) 1.
[2] J.J. Petrovic, Mater. Res. Bull. 18 (1993) 35.
[3] J.J. Petrovic, Mater. Sci. Eng. A 192/193 (1995) 31.
[4] J.J. Petrovic, A.K. Vasudevan, Mater. Sci. Eng. A 261 (1999) 1.
[5] M. Henzel, J. Kovalcik, J. Dusza, A. Juhasz, J. Lendvai, J. Mater. Sci. 39 (2004) 3769.
[6] J. Xu, H. Zhang, G. Jiang, B. Zhang, W. Li, Trans. Nonferr. Met. Soc. China 16 (2006) s504.
[7] L. Sun, J. Pan, Mater. Lett. 52 (2002) 223.
[8] J.M.E. Harper, K.P. Rodbell, J. Vac. Sci. Technol. B 15 (1997) 763.
[9] C.H. Ho, Y.H.C. Cha, S. Prakash, G. Potwin, H.J. Doerr, C.V. Deshpandey, R.F. Bunshah, M. Zeller, Thin Solid Films 260 (1995) 232.
[10] T.P. Thorpe, A.A. Morrish, S.B. Qadri, J. Vac. Sci. Technol. A 7 (1989) 1279.
[11] S. Inoue, N. Toyokura, T. Nakamura, M. Maeda, M. Takagi, J. Electrochem. Soc. 130 (1983) 1603.
[12] G.A. West, K.W. Beeson, J. Electrochem. Soc. 135 (1988) 1752.
[13] S. Madhukar, S. Aggarwal, A.M. Dhote, R. Ramesh, S.B. Samavedam, S. Choopun, R.P. Sharma, J. Mater. Res. 14 (1999) 940.
[14] R. Teghil, A. Giardini Guidoni, A. Mele, S. Piccirillo, M. Coreno, V. Marotta, T.M. Di Palma, Surf. Interface Anal. 22 (1994) 181.
[15] R. Felici, F. Colloco, R. Caminiti, C. Sadun, V. Rossi, Italian Patent No. RM 93 A 000410, 1993.
[16] B. Paci, A. Generosi, V. Rossi Albertini, E. Agostinelli, G. Varvaro, D. Fiorani, Chem. Mater. 16 (2004) 292.
[17] D. Ferro, R. Scandurra, A. Latini, J.V. Rau, S.M. Barinov, J. Mater. Sci. 39 (2004) 329.
[18] D. Ferro, J.V. Rau, V. Rossi Albertini, A. Generosi, R. Teghil, Surf. Coat. Technol. 202 (2008) 1455.
[19] B. Joensson, S. Hogmark, Thin Solid Films 114 (1984) 257.
[20] A. Iost, R. Bigot, Surf. Coat. Technol. 80 (1996) 117.
[21] F. Froehlich, P. Grau, W. Grellmann, Phys. Status Solidi A 42 (1977) 79.
[22] A.M. Korsunsky, M.R. McGurk, S.J. Bull, T.F. Page, Surf. Coat. Technol. 99 (1998) 171.
[23] E.S. Puchi-Cabrera, Surf. Coat. Technol. 160 (2002) 177.
[24] L.F. Mattheiss, Phys. Rev. B 45 (1992) 3252.
[25] J.V. Rau, A. Generosi, V.V. Smirnov, D. Ferro, V. Rossi Albertini, S.M. Barinov, Acta Biomater. 4 (2008) 1089.
[26] R. Teghil, L. D'Alessio, A. Santagata, M. Zaccagnino, D. Ferro, Appl. Surf. Sci. 186 (2002) 335.
[27] D.G. Morris, M. Leboeuf, M.A. Morris, Mater. Sci. Eng. A 251 (1998) 262.
[28] Y. Qiao, H. Zhang, C. Hong, X. Zhang, J. Phys., D, Appl. Phys. 42 (2009) 105413/1.
[29] R.A. Andrievski, Int. J. Refract. Met. Hard Mater. 19 (2001) 447.